nature structural & molecular biology

Structure of the Rpn11–Rpn8 dimer reveals mechanisms of substrate deubiquitination during proteasomal degradation

Evan J Worden[1], Chris Padovani[1] & Andreas Martin[1,2]

Polyubiquitin chains target protein substrates to the 26S proteasome, where they are removed by the deubiquitinase Rpn11 to allow efficient substrate degradation. Despite Rpn11's essential function during substrate processing, its detailed structural and biochemical characterization has been hindered by difficulties in purifying the isolated enzyme. Here we report the 2.0-Å crystal structures of Zn^{2+}-free and Zn^{2+}-bound *Saccharomyces cerevisiae* Rpn11 in an MPN-domain heterodimer with Rpn8. The Rpn11-Rpn8 interaction occurs via two distinct interfaces that may be conserved in related MPN-domain complexes. Our structural and mutational studies reveal that Rpn11 lacks a conserved surface to bind the ubiquitin Ile44 patch, does not interact with the moiety on the proximal side of the scissile isopeptide bond and exhibits no linkage specificity for ubiquitin cleavage. These findings explain how Rpn11 functions as a promiscuous deubiquitinase for cotranslocational substrate deubiquitination during proteasomal degradation.

© 2014 Nature America, Inc. All rights reserved.

The ubiquitin proteasome system is responsible for strictly regulated ATP-dependent protein degradation in all eukaryotic cells[1,2]. In this process, damaged, misfolded or obsolete proteins are marked for degradation by condensation of one or several of their lysine side chains with the C terminus of ubiquitin to form an isopeptide linkage[3]. Polyubiquitination, which is required for degradation by the 26S proteasome, occurs when additional ubiquitin moieties are attached to any of the seven lysine residues within ubiquitin itself, to form chains with different linkage types. Ubiquitin chains linked through Lys11, Lys48 and potentially Lys63 target substrate proteins to the 26S proteasome[4–6], where before degradation the ubiquitin chains are removed by deubiquitinases (DUBs) that cleave the isopeptide bonds.

The 26S proteasome is a 2.5-MDa molecular machine composed of at least 34 different proteins, 11 of which have enzymatic activities[7]. It can be biochemically separated into three subcomplexes: the core peptidase, the base and the lid[8]. The core peptidase consists of four stacked heptameric rings that form a proteolytic chamber with sequestered active sites accessible only to unfolded polypeptides through gated axial pores[9,10]. The base is made from nine subunits, six of which are AAA+ ATPases that form a heterohexameric ring and constitute the molecular motor of the proteasome[11]. This ATPase ring binds to the axial surface of the core and translocates protein substrates into the degradation chamber after mechanically unraveling their folded structures[12–16]. The lid sits on one side of the base and is composed of ten subunits, including the only essential DUB of the proteasome, Rpn11 (refs. 17,18). During degradation, condemned proteins are tethered by their polyubiquitin modification to an intrinsic ubiquitin receptor within the lid or the base, before a flexible segment of their structure is engaged by the translocation machinery of the base ATPase ring[19]. Removal of attached ubiquitins by Rpn11 is then required for efficient substrate translocation through the narrow axial pore into the peptidase[17].

Rpn11 is a Zn^{2+}-dependent DUB of the JAMM- and MPN-protein family[17,18]. Many MPN-domain proteins have highly divergent insertion sequences, termed Insert-1 (Ins-1) and Insert-2 (Ins-2), which intervene in the core MPN fold[20]. The Ins-1 region of JAMM DUBs has been suggested to function in both recognizing the distal ubiquitin in a diubiquitin substrate and correctly positioning the distal-ubiquitin C terminus over the DUB active site for isopeptide-bond cleavage (**Fig. 1a**). In contrast, the Ins-2 region seems to determine the DUB specificity for a certain ubiquitin linkage type by interacting with the proximal ubiquitin. For instance, in the Rpn11-related DUB AMSH-LP the Ins-2 region contacts the proximal moiety of Lys63-linked diubiquitin[20]. Throughout this paper, we will refer to the moieties on either side of a scissile isopeptide bond as 'distal' and 'proximal'. The distal moiety presents its C-terminal glycine to the DUB active site, and the proximal moiety is bound through its isopeptide-linked lysine (**Fig. 1a**).

Cryo-EM studies of the proteasome holoenzyme revealed that Rpn11 forms a dimer with Rpn8, the only other proteasomal MPN-domain protein, and is located directly above the central pore leading into the N-terminal-domain ring (N ring) of the base ATPases[21–23]. Owing to steric restrictions imposed by this proximity to the base N ring, Rpn11 may be prevented from cleaving between ubiquitin moieties. The enzyme in the proteasome context seems to remove chains *en bloc* by hydrolyzing the isopeptide bond between a substrate lysine and the

[1]Department of Molecular and Cell Biology, University of California, Berkeley, Berkeley, California, USA. [2]California Institute for Quantitative Biosciences, University of California, Berkeley, Berkeley, California, USA. Correspondence should be addressed to A.M. (a.martin@berkeley.edu).

Received 1 November 2013; accepted 15 January 2014; published online 23 January 2014; doi:10.1038/nsmb.2771

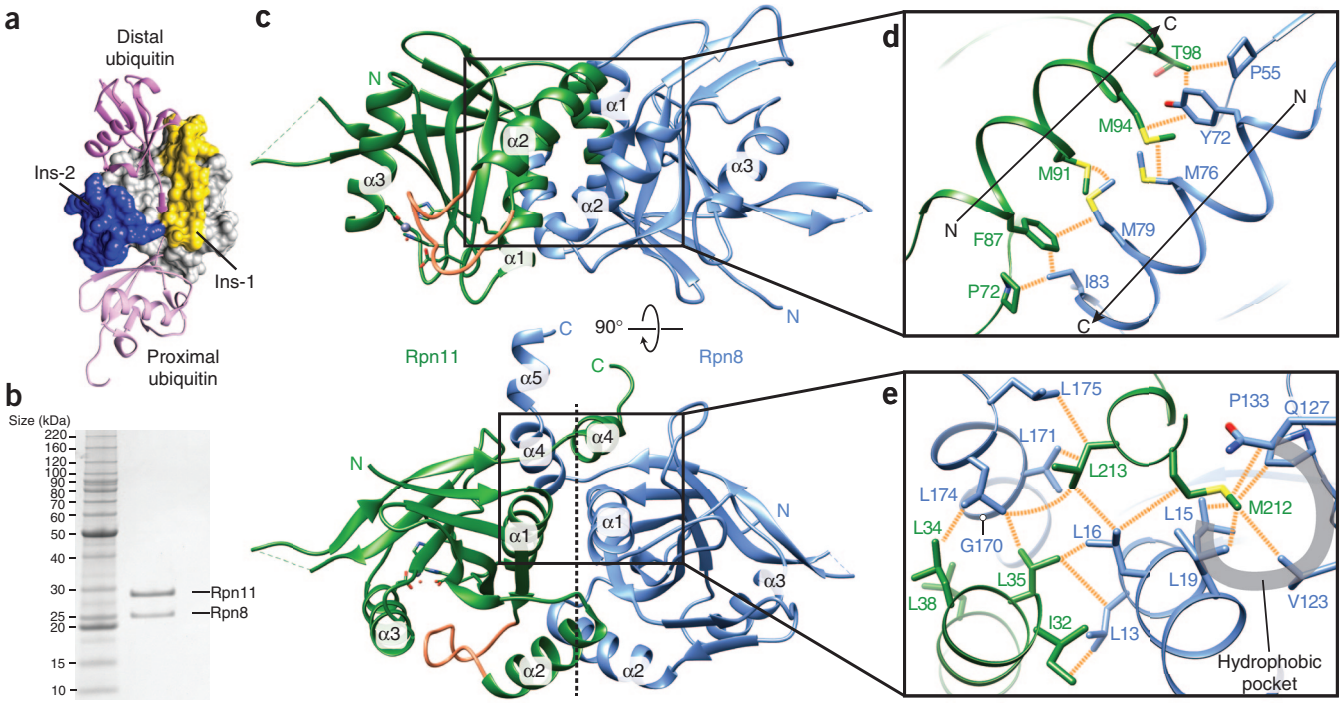

Figure 1 Rpn11 and Rpn8 form a heterodimer through two distinct interfaces. (**a**) Structure of the Rpn11-related DUB AMSH-LP, highlighting the proximal and distal moieties of a bound Lys63-linked diubiquitin substrate as well as the Ins-1 and Ins-2 segments involved in binding. Distal refers to the moiety whose C-terminal glycine forms the isopeptide linkage with the lysine in the proximal moiety. (**b**) Coomassie-stained SDS-PAGE gel of the purified Rpn11–Rpn8 heterodimer. Rpn11 gave reproducibly better staining despite its 1:1 stoichiometry with Rpn8. (**c**) Structure of the Rpn11–Rpn8 heterodimer, shown in two orientations rotated by 90° with respect to each other. Rpn11 and Rpn8 are colored green and blue, respectively, and the Ins-1 loop of Rpn11 is colored orange. Zn^{2+}-coordinating residues of the Rpn11 active site are shown in stick representation. The α-helices in Rpn11 and Rpn8 are labeled α1–α4 and α1–α5, respectively (with α5 formed by four additional residues left behind after PreScission cleavage of the purification tag). In the bottom image, the dashed line indicates the pseudo–two-fold axis of rotation between Rpn11 and Rpn8. (**d**) Close-up view showing the structure of Rpn11–Rpn8 dimerization interface 1. Hydrophobic interactions are shown by orange dashed lines. The helices of interface 1 are arranged in an antiparallel orientation denoted by the black arrows. (**e**) Close-up view showing the structure of interface 2. Hydrophobic interactions are indicated with orange dashed lines. A gray horseshoe emphasizes the hydrophobic pocket in Rpn8 that accommodates Met212 of Rpn11.

© 2014 Nature America, Inc. All rights reserved.

C terminus of the first ubiquitin[18], but it remains unknown whether cleavage can also occur between ubiquitin moieties or whether the enzyme exhibits any linkage-type specificity[24].

Deubiquitination by Rpn11 has been shown to depend on ATP hydrolysis by the base and may thus be tightly linked to the other degradation steps of substrate engagement, unfolding and translocation[17,18]. One model predicts that the ATPase-driven translocation of a protein substrate pulls the isopeptide bonds of attached ubiquitin modifications into the Rpn11 active site for cleavage. However, this complicated set of coupled processes has so far strongly hindered detailed mechanistic studies of this DUB in the proteasome context. Furthermore, Rpn11 has proven over many years to be extremely recalcitrant to purification, thus making biochemical and structural studies of the isolated enzyme impossible. These obstacles have also prevented the development of potent inhibitors for Rpn11, which is an attractive drug target for attenuation of proteasomal degradation.

To obtain high-resolution structural and mechanistic insights, we optimized the Rpn11–Rpn8 heterodimer from *S. cerevisiae* for crystallization and functional characterization *in vitro*. Here we present the 2.0-Å-resolution crystal structure of this heterodimer. Unexpectedly, the structure reveals that the Rpn11 catalytic groove lacks several features that are conserved in related DUBs and were predicted to be critical for ubiquitin binding or stabilization of the isopeptide bond for cleavage. Rpn11 is missing an important aromatic residue thought to contact the hydrophobic Ile44 patch of ubiquitin, and it uses a flexible Ins-1 loop rather than an extended β-sheet to position the C terminus of the distal ubiquitin moiety for cleavage. Furthermore, Ins-2 is not involved in stabilizing the isopeptide bond above the active site but instead contacts the non-ATPase subunit Rpn2 of the base and thereby probably anchors Rpn11 within the proteasome complex. Rpn11 thus differs substantially from related DUBs in its mode of ubiquitin interaction, consistent with Rpn11 deubiquitination occurring concomitantly with substrate translocation.

RESULTS

Purification of the Rpn11–Rpn8 heterodimer

Our laboratory and others have suggested that Rpn11 and Rpn8 form a dimer within the proteasome lid and that this dimerization occurs through an interface between the MPN domains of the two proteins[21,25]. Furthermore, we have shown previously that the lid subcomplex is assembled through the formation of a large helical bundle consisting of the C-terminal helices of all lid subunits including Rpn8 and Rpn11 (refs. 25,26). We thus reasoned that the numerous previous attempts to purify Rpn11 in isolation were unsuccessful because its MPN dimerization surface was unsaturated and its C-terminal helices were not paired with others in the helical bundle. To get around this problem, we coexpressed C-terminally truncated variants of Rpn11 (residues 2–239) and Rpn8 (residues 1–179), which contained only their respective MPN domains (hereafter referred to as Rpn11 and Rpn8) and affinity tags for purification. Using this coexpression construct, we were able to purify DUB-active Rpn11–Rpn8 heterodimers to high purity and yield (**Fig. 1b**).

Structure of the Rpn11–Rpn8 heterodimer

We obtained crystals of the Rpn11–Rpn8 heterodimer complex from proteins purified under conditions in which the catalytic Zn^{2+} ion was stripped from Rpn11, which thus formed an apoenzyme complex. We collected X-ray diffraction data not only on these apoenzyme crystals but also on the active Zn^{2+}-bound complex, after soaking crystals in Zn^{2+}-containing mother liquor (**Table 1**). We accomplished molecular replacement by using Csn5 (PDB 4F7O[26]) and Mov34 (PDB 2O95 (ref. 27)) as search models for Rpn11 and Rpn8, respectively. Apart from the appearance of electron density for Zn^{2+} in the Rpn11 active site (**Supplementary Fig. 1**), the structure of the Zn^{2+}-bound Rpn11–Rpn8 heterodimer did not show any major structural differences when compared to the apoenzyme complex. In addition, residues around the active site of Rpn11, both in the apo and Zn^{2+}-bound states, are nicely superimposable with the structure of the related DUB AMSH-LP with bound diubiquitin, thus further confirming that our Rpn11 structure represents an active, functionally relevant conformation.

MPN domains in multiprotein complexes generally show a high propensity for dimer formation[26,27]. However, available crystal structures of MPN dimers exhibit considerable variation in the mode of dimerization, and it has remained unclear which of the observed interactions, if any, are physiologically relevant. The structure of the Rpn8–Rpn11 heterodimer presented here now reveals an interaction in which the two MPN domains are rotated relative to each other around a pseudo–two-fold axis, in a manner reminiscent of the Rpn8 homodimer structure[27] (**Fig. 1c**). The dimerization of Rpn11 and Rpn8 is primarily based on interactions between α-helices that form two distinct interfaces, interface 1 and interface 2, which have a combined buried surface area of ~4,100 $Å^2$ (**Fig. 1c–e**). Interface 1, located between Rpn11 α2 and Rpn8 α2, is formed around a cluster of four methionines: Met91 and Met94 of Rpn11 and Met79 and Met76 of Rpn8. Flanking this methionine cluster are other hydrophobic interactions: the γ carbon of Rpn11 Thr98 interacts with the aliphatic side chains of Rpn8 Pro55 and Tyr72, and the ε carbon of Rpn8 Ile83 interacts with Rpn11 Phe87 and Pro72 (**Fig. 1d**). Interestingly, the helices of interface 1 pack in an antiparallel orientation, and the interacting residues are closely matched between the two proteins, thus emphasizing the overall pseudo–two-fold symmetry of the entire complex.

Interface 2 primarily consists of a four-helix bundle formed between α1 and α4 of Rpn11 and α1 and α4 of Rpn8. In a swap-like arrangement, α4 of Rpn11 and α4 of Rpn8 reach across the interface, and each interacts tightly with the MPN domain of the other protein (**Fig. 1c**,**e**). The four-helix bundle has a tightly packed hydrophobic core rich in leucine residues. In particular, Leu35 and Leu213 of Rpn11 and Leu174 and Leu16 of Rpn8 are involved in numerous hydrophobic contacts and compose the center of the hydrophobic core (**Fig. 1e**). Interestingly, Rpn11 Met212 packs into a very tight hydrophobic pocket formed by Rpn8 Pro133, Gln127, Val123, Leu19, Leu15 and Leu16. The residue in Rpn8 corresponding to Rpn11 Met212 (related by the pseudo–two-fold symmetry of the complex) is Gly170, which packs very tightly against Rpn11 Leu34, Leu35 and Leu38 (**Supplementary Fig. 2**). This substantial size difference between corresponding residues at the interface probably facilitates heterodimer formation and may explain why homodimers of only Rpn8 and not Rpn11 are observed as byproducts of the coexpression. The hydrophobic pocket that accommodates Rpn11 Met212 in the heterodimer with Rpn8 would not exist in an Rpn11 homodimer. Packing of this residue against Rpn11 Leu34, Leu35 and Leu38 would therefore lead to major steric clashes that preclude Rpn11-homodimer formation.

Five multiprotein complexes in humans that contain pairs of JAMM- or MPN-domain proteins have so far been identified: the lid of the 26S proteasome, the COP9 signalosome, eIF3, BRISC and BRCA1-A[28–31]. An increasing body of evidence suggests that the MPN-domain proteins in these complexes have an intrinsic ability to form dimers. Furthermore, sequence alignments of Rpn11 and Rpn8 with their cognate JAMM- and MPN-domain counterparts in these complexes reveal that the residues making up the hydrophobic cores of the dimer interfaces 1 and 2 are chemically well conserved, despite a strong divergence in primary sequence (**Supplementary Figs. 3** and **4**). It thus seems likely that the Rpn11-Rpn8 interaction represents a general mode of dimerization that may be recapitulated in at least a subset of other JAMM- and MPN-domain containing complexes and may have a role in positioning the respective subunits for their catalytic or scaffolding functions.

Table 1 Data collection and refinement statistics

	Zn^{2+}-bound Rpn11–Rpn8	Zn^{2+}-free Rpn11–Rpn8
Data collection		
Space group	$P4_32_12$	$P4_32_12$
Cell dimensions		
a, *b*, *c* (Å)	70.296, 70.296, 198.912	70.405, 70.405, 198.887
Resolution (Å)	48.23–1.991 (2.02–1.99)[a]	40.615–1.950 (1.98–1.950)
R_{sym}	0.076 (0.710)	0.075 (NA)
$I / \sigma I$	20.62 (3.40)	20.99 (3.62)
Completeness (%)	99.33 (98.31)	92.56 (72.00)
Redundancy	8.1 (8.3)	11.9 (12.0)
Refinement		
Resolution (Å)	48.23–1.991	40.615–1.950
No. reflections	34,915	37,562
R_{work} / R_{free}	0.161 / 0.1951	0.1626 / 0.2094
No. atoms	3,082	3,069
Protein	2,702	2,714
Ligand/ion	125	84
Water	255	271
B factors		
Protein	35.50	27.20
Ligand/ion	55.60	44.90
Water	44.00	34.70
r.m.s. deviations		
Bond lengths (Å)	0.013	0.014
Bond angles (°)	1.33	1.39

[a]Values in parentheses are for highest-resolution shell. NA, not applicable

Rpn11 lacks predicted residues for ubiquitin binding

Previous structural studies on the related DUB, AMSH-LP, revealed that its interface for binding to the hydrophobic patch around Ile44 of ubiquitin is composed of two surface residues, Val328 and Phe332 (ref. 20). These residues seemed to align well with Rpn11 Val83 and Phe87, respectively, and on the basis of this apparent conservation it had been proposed that Rpn11 binds the Ile44 patch of ubiquitin in a manner very similar to that of AMSH-LP (**Fig. 2a**). However, our structure-based alignment between Rpn11 and AMSH-LP revealed that Rpn11 displays Asp85 and Ala89, rather than Val83 and Phe87, at the positions predicted to be critical for ubiquitin binding (**Fig. 2a**,**b** and **Supplementary Fig. 5**). Strikingly, Phe87 is involved in forming interface 1 with Rpn8, thus making this residue completely inaccessible for ubiquitin binding (**Fig. 2b**).

On the basis of the observed sequence differences, we predicted Rpn11's K_m for diubiquitin cleavage to be much higher than that of AMSH-LP. Surprisingly, using a gel-based assay for the cleavage of Lys48-linked diubiquitin, we found that Rpn11 has a K_m of ~120 μM,

© 2014 Nature America, Inc. All rights reserved.

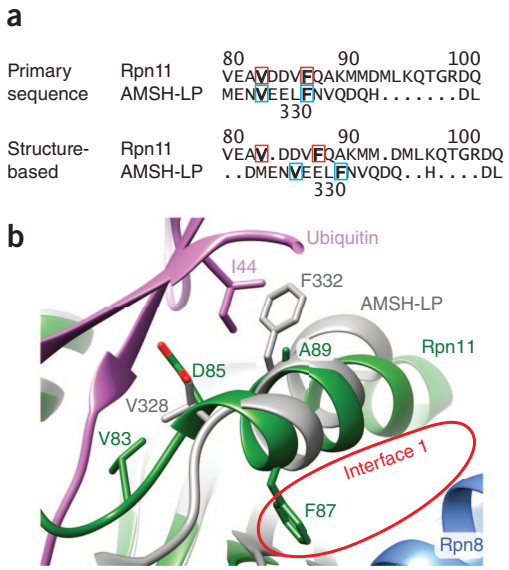

Figure 2 Rpn11 is missing a conserved binding site for the Ile44 patch of ubiquitin. (**a**) Sequence alignments between the helical Ins-1 region of Rpn11 and AMSH-LP. Top, primary-sequence alignment, with the ubiquitin-interacting residues of AMSH-LP highlighted in blue and the previously proposed corresponding residues of Rpn11 highlighted in red. Bottom, structure-based alignment showing a two-residue offset between Rpn11 and AMSH-LP. (**b**) Structure of the predicted ubiquitin-binding surface of Rpn11. Rpn11 and Rpn8 are shown in green and blue, respectively. The crystal structure of ubiquitin-bound AMSH-LP[20] (PDB 2ZNV; AMSH-LP in gray, ubiquitin in pink) is superimposed with the structure of Rpn11. AMSH-LP residues involved in the binding of the ubiquitin Ile44 patch are shown in stick representation. Residues at the corresponding positions in Rpn11 as well as residues previously predicted to bind ubiquitin are also shown as sticks.

which is only 70% higher than the K_m of ~72 μM for AMSH-LP (**Table 2** and **Supplementary Fig. 6**). Because Rpn11 appeared to lack hydrophobic residues conserved in AMSH-LP to bind the Ile44 patch of ubiquitin, we sought to characterize its mode of ubiquitin binding in more detail. If Rpn11 binds ubiquitin in a similar orientation as does AMSH-LP, reconstructing an AMSH-LP-like binding surface in Rpn11 would be expected to lower the K_m for diubiquitin cleavage. To test this hypothesis, we generated the mutants Rpn11^{A89F} and Rpn11^{D85V}. The A89F mutation decreased the K_m 3.4-fold (**Table 2**), indicating that wild-type Rpn11 indeed binds the distal ubiquitin in a similar orientation as does AMSH-LP, but it lacks hydrophobic residues thought to be required for tight interaction with the Ile44 hydrophobic patch. In contrast, the D85V mutation led to a 1.7-fold increase in K_m relative to that of wild type, suggesting that a valine residue in this position of Rpn11 does not favorably contribute to ubiquitin binding. Moreover, this mutation decreased the k_{cat} for diubiquitin cleavage to 27% (**Table 2**), possibly by affecting the orientation of the distal ubiquitin and thus the positioning of the isopeptide bond in the Rpn11 active site. Consistently with our data, this valine residue is not well conserved among JAMM DUBs or even within the AMSH family of proteins[20,32], despite being implicated in AMSH-LP binding to the Ile44 patch of ubiquitin.

Together, these results indicate that Rpn11 and AMSH-LP bind ubiquitin in a similar orientation but differ considerably in their interactions with the Ile44 hydrophobic patch. Ubiquitin-binding affinity of Rpn11 can therefore be increased by the reengineering of a critical phenylalanine present at the equivalent position in AMSH-LP. In contrast to the lack of this phenylalanine, Rpn11 contains other conserved or highly similar residues that have been shown to mediate ubiquitin binding in AMSH-LP. For instance, Rpn11 displays Leu132 in the same position as AMSH-LP Met370, the latter of which makes important interactions with the hydrophobic pocket formed by Ile36, Leu69 and Leu71 of ubiquitin. Indeed, the Leu132A mutation in Rpn11 leads to a 2.6-fold increase in K_m and a 5.4-fold decrease in k_{cat} for diubiquitin cleavage, results indicating that this residue is important for both ubiquitin binding and isopeptide-bond hydrolysis (**Table 2**).

Ins-2 of Rpn11 is not involved in ubiquitin binding

Rpn11 contains both Ins-1 and Ins-2, but Ins-2 is not ordered in our structure of the isolated Rpn11–Rpn8 dimer. The absence of a defined conformation may be caused by the lack of Zn^{2+}-coordinating residues in the Ins-2 of Rpn11. In AMSH-LP, these Zn^{2+}-binding residues appear to structure Ins-2 and allow its interaction with the proximal ubiquitin[20]. Docking of the Rpn11 crystal structure into the EM density of the substrate-bound proteasome holoenzyme[22] indicates that Ins-2, together with the Rpn11 N terminus, interacts with Rpn2 and helps position Rpn11 above the proteasome pore (**Supplementary Fig. 7**). Thus, the role of the Ins-2 region in Rpn11 seems completely distinct from that in AMSH-LP. Because a defined conformation of the Rpn11 Ins-2 may depend on its interactions with Rpn2, it is not surprising that this segment is unresolved in the structure of the isolated Rpn11–Rpn8 dimer.

Our crystal structure, in combination with the proteasome EM reconstruction, clearly indicates that Rpn11 lacks the interfaces for contacting the proximal moiety of a bound diubiquitin, an interaction that would be required to confer linkage specificity. Docking of diubiquitin into Rpn11, with the scissile isopeptide bond placed at the active site, shows that the proximal ubiquitin is completely exposed (**Fig. 3a**). Using diubiquitin cleavage assays

Table 2 Kinetic parameters for the cleavage of Lys48- or Lys63-linked diubiquitin by wild-type or mutant Rpn11 in context of the Rpn11–Rpn8 heterodimer

Rpn11 (in Rpn8 context)	Ub_2 linkage type	K_m (μM)	k_{cat} (min^{-1})
WT	48	120 ± 28	0.29 ± 0.11
WT	63	299 ± 52	0.38 ± 0.05
WT	11	147 ± 43	0.74 ± 0.20
WT	Ubiquitin-lysine-TAMRA	20 ± 1	0.95 ± 0.02
A89F	48	36 ± 7	0.25 ± 0.06
D85V	48	205 ± 43	0.08 ± 0.01
L132A	48	320 ± 36	0.07 ± 0.01
V78A	48	142 ± 41	0.20 ± 0.07
S79A	48	218 ± 50	0.13 ± 0.01
V80A	48	(K_d = 67 ± 35)	ND
E81A	48	515 ± 96	0.11 ± 0.01
Δ78–81	48	ND	ND
78–81 AAAA	48	ND	ND

ND, not detectable. K_m and k_{cat} values for diubiquitin hydrolysis by wild-type (WT) or mutant Rpn11 were determined by Michaelis–Menten analyses, with 5 μM of Rpn11–Rpn8 and a gel-based assay to follow cleavage (Online Methods). The K_d value for diubiquitin binding to the catalytically inactive Rpn11^{V80A} was measured by the change in tryptophan fluorescence. K_m and k_{cat} values for ubiquitin-lysine-TAMRA cleavage were determined with a fluorescence-polarization assay with Rpn11–Rpn8 at 250 nM and 1.25 μM and ubiquitin-lysine-TAMRA concentrations ranging from 1 to 10 μM (Online Methods). All reported values are the average of three measurements ± s.d. (n = 3 technical repeats).

© 2014 Nature America, Inc. All rights reserved.

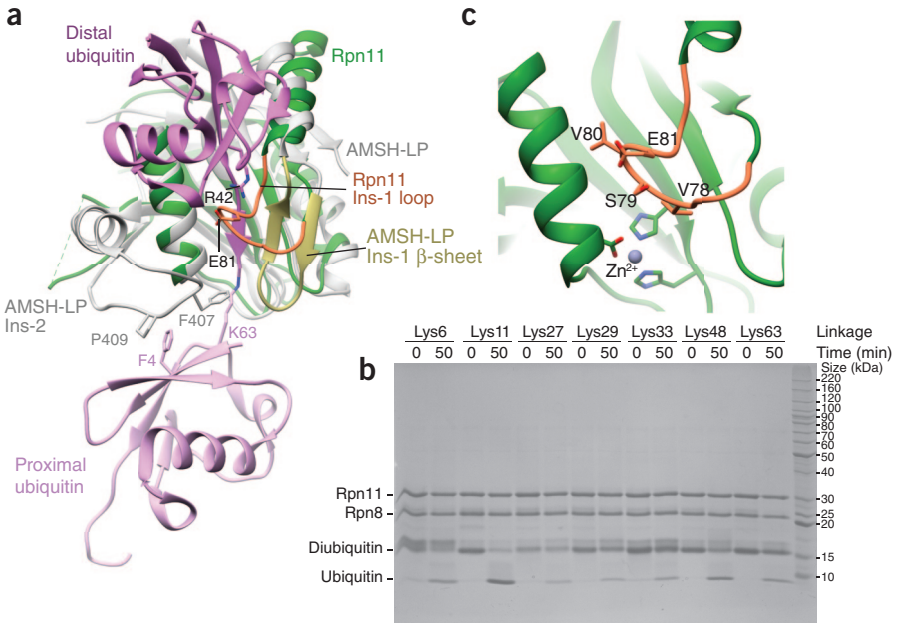

Figure 3 Missing proximal contacts allow Rpn11 cleavage promiscuity. (**a**) Superimposition of the crystal structures for ubiquitin-bound AMSH-LP (gray; PDB 2ZNV) and Rpn11 (green). The Ins-1 segments involved in stabilizing the ubiquitin C terminus in the catalytic groove are shown in orange for Rpn11 and yellow for AMSH-LP. Residues that mediate the interaction between AMSH-LP Ins-2 and the proximal ubiquitin are shown as sticks. In Rpn11, Ins-2 is relocated away from the proximal ubiquitin to interact with Rpn2 (**Supplementary Fig. 7**). Potentially interacting residues between the Rpn11 Ins-1 loop and the distal ubiquitin (Glu81 and Arg42) are also shown in stick representation. (**b**) Rpn11 cleavage of multiple diubiquitin linkage types. Shown is a Coomassie-stained SDS-PAGE gel detailing Rpn11 cleavage of Lys6-, Lys11-, Lys27-, Lys29-, Lys33-, Lys48- and Lys63-linked diubiquitin. (**c**) Structure of the Rpn11 catalytic site, oriented as in **a**. The Ins-1 loop (colored orange) covers the binding groove and is shown with individually mutated residues in stick representation. The Zn^{2+}-coordinating residues of Rpn11 are also in stick representation.

(**Fig. 3b** and **Supplementary Fig. 6**), we accordingly found that Rpn11 does not exhibit linkage specificity in its deubiquitination activity. Isolated Rpn11 efficiently cleaves all seven ubiquitin linkage types (**Fig. 3b**). Lys11-, Lys48- and Lys63-linked diubiquitins are cleaved with k_{cat} values of 0.74, 0.29 and 0.38 min^{-1}, respectively, and K_m values of 147, 120 and 299 μM, respectively (**Table 2**). The relatively small differences in K_m and k_{cat} are presumably a consequence of the different linkage types forming variable compact ubiquitin-chain conformations that make the isopeptide bond transiently inaccessible. It has been shown previously that these conformations 'breathe' and expose the isopeptide bond with different frequencies, thus leading to variations in DUB cleavage rates[33]. Moreover, depending on the linkage type, steric clashes between the proximal ubiquitin and Rpn11 may influence the K_m. Another factor that is likely to affect K_m and k_{cat} for cleavage of isolated diubiquitin is the extent of nonproductive binding, in which the first, proximal moiety interacts with the distal site of the Rpn11-binding groove and thus competitively inhibits isopeptide-bond cleavage between ubiquitin moieties. Because a modification on Lys63 of a distally bound ubiquitin probably leads to fewer steric clashes with Rpn11 than does a modification on Lys48 or Lys11, the proximal ubiquitin of isolated Lys63-linked diubiquitin may be a better competitive inhibitor than the proximal ubiquitin in other linkage types. This could explain the higher K_m for Lys63-linked diubiquitin despite its reportedly less compact and more extended conformation. Importantly, for deubiquitination during proteasomal degradation such competitive inhibition would not exist because the ubiquitin chain would be attached to a protein substrate as the proximal moiety.

To assess whether the identity or folding state of the moiety proximal to the isopeptide bond affects K_m as well as k_{cat}, we measured Rpn11 cleavage of ubiquitin-lysine-TAMRA (**Table 2** and **Supplementary Fig. 8a–c**). The determined K_m of ~20 μM is 6- to 15-fold lower than the K_m values for Lys11-, Lys48- or Lys63-linked diubiquitin, a result consistent with our model that a globular structure on the proximal side of the isopeptide bond leads to some steric hindrance in Rpn11 binding. Therefore, Rpn11 apparently does not make favorable interactions with a proximal ubiquitin, and this is in agreement with the observed lack of cleavage within ubiquitin chains. The k_{cat} of 1 min^{-1} for ubiquitin-lysine-TAMRA is very similar to the k_{cat} values for diubiquitin. This similarity indicates that in its catalysis Rpn11 does not discriminate the identity or folding state of the molecule on the proximal side of the scissile bond. This is in excellent agreement with Rpn11's promiscuous function in the proteasome context, in which it removes ubiquitin chains from highly variable protein substrates. Steric restrictions by the neighboring base N ring appear to preclude larger folded domains, including ubiquitin, from the proximal side of the scissile bond, such that Rpn11 is assumed to cleave only at the base of the ubiquitin chain, between the substrate lysine and the very first ubiquitin. The variable compactness of different ubiquitin chain types would therefore have no effect on the accessibility of the cleaved isopeptide bond and the rate of deubiquitination at the proteasome. Potential K_m differences that originate from different linkage types on the ubiquitin bound to the distal site of Rpn11 are also likely to be irrelevant because ubiquitin chains are tethered to intrinsic proteasome receptors with high affinity that substantially increase the local substrate concentration.

Flexible Ins-1 loop positions distal ubiquitin for cleavage

Our structural data suggest that Rpn11 binds its ubiquitin substrates exclusively by contacting the distal side of the isopeptide bond. Interestingly, the Ins-1 region of Rpn11 includes a prominent loop that sits over the ubiquitin-binding groove, approximately 12 Å away from the active site residues (**Fig. 3c**). This loop has high *B* factors, indicating that it has some level of intrinsic flexibility. The position of the Ins-1 loop over the catalytic groove could suggest that it blocks access for the ubiquitin C terminus and thereby fulfills an autoinhibitory function to reduce spurious isopeptide cleavage, similarly to a mechanism proposed for Csn5 in the COP9 signalosome[26]. On the basis of this model, deletion of residues from the Rpn11 Ins-1 loop should increase isopeptide-cleavage activity by exposing the catalytic groove for ubiquitin binding. However, we found that deletion of the highly conserved residues 78–81 in the $Rpn11^{\Delta 78-81}$ mutant completely abolished DUB activity (**Table 2**). Similarly, a mutant with residues 78–81 replaced by alanines lacked detectable activity, thus ruling out that the defects observed for the loop truncation were simply caused by a strained conformation with a distorted active site. Consequently, the Ins-1 loop of Rpn11 does not act in an inhibitory fashion but rather seems to be required for catalysis.

© 2014 Nature America, Inc. All rights reserved.

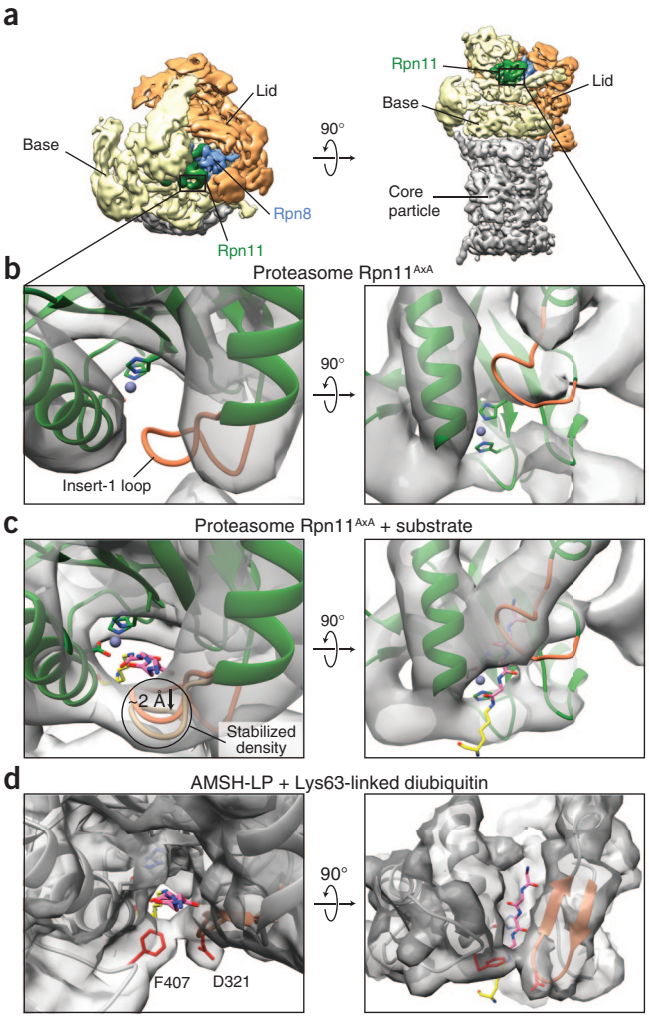

Figure 4 The Ins-1 loop of Rpn11 acts as a flap to fold over the ubiquitin C terminus. (**a**) EM three-dimensional reconstruction of the proteasome holoenzyme as shown from the top (left) and front (right). Rpn11 and Rpn8 are shown in green and blue. The lid, base and core-particle subcomplexes are shown in orange, tan and gray, respectively. (**b**) Close-up views of the crystal structure of Rpn11 docked into the EM reconstruction of substrate-free yeast proteasomes with catalytically dead Rpn11 (Rpn11AxA[22]) as viewed from the top (left) and front (right). (**c**) Close-up views of the Rpn11 structure docked into the EM reconstruction of Rpn11^{AxA}-mutant proteasomes stalled on an ubiquitinated substrate[22], again viewed from the top and front. The backbone for the C-terminal portion of the distal ubiquitin (Leu-Arg-Gly-Gly; pink) and the side chain for the isopeptide-linked lysine (yellow), were docked on the basis of the ubiquitin-bound model of Rpn11 and are shown in stick representation. In addition to the rigid-body fit of the entire Rpn11, including the Ins-1 loop (orange), we manually docked the isolated loop (yellow) to fit even better into the observed EM density. (**d**) Close-up views of the ubiquitin-bound AMSH-LP crystal structure (PDB 2ZNV) with its simulated EM-density envelope and the C-terminal Leu-Arg-Gly-Gly-Lys peptide (pink and yellow sticks) are shown in orientations similar to those of Rpn11 in **b** and **c**. Residue Asp321 of Ins-1 and residue Phe407 of Ins-2 form a bridge over the active site and are depicted as red sticks.

To determine whether interactions of this loop with ubiquitin contribute primarily to K_m or k_{cat}, we individually mutated residues 78–81 to alanine and measured the cleavage of Lys48-linked diubiquitin (**Table 2**). Rpn11^{V78A} did not considerably differ from the wild-type enzyme, whereas Rpn11^{S79A} and Rpn11^{E81A} showed an ~1.8- and ~4.3-fold increase in K_m, respectively, and a ~2.2- and ~2.6-fold decrease in k_{cat}, respectively. Importantly, the V80A mutation completely eliminated diubiquitin cleavage. Using a tryptophan fluorescence–based ubiquitin binding assay, we found that the K_d of Rpn11^{V80A} is similar to or even slightly lower than the K_m of wild-type Rpn11 (**Table 2** and **Supplementary Fig. 8d**). This indicates that the observed lack of cleavage activity for this mutant originates from a severe defect in k_{cat}. The Ins-1 loop may thus have an important role in positioning the C terminus of the distal ubiquitin for isopeptide-bond cleavage.

The corresponding Ins-1 region in AMSH-LP does not adopt a loop conformation but forms a short two-stranded β-sheet in the absence of ubiquitin. This β-sheet defines one edge of the catalytic groove and stabilizes a bound substrate for cleavage by forming a three-stranded sheet with the C terminus of the distal ubiquitin. Because Rpn11 and AMSH-LP appear to bind the distal ubiquitin in a similar orientation, we superimposed their crystal structures to generate a model for ubiquitin-bound Rpn11 (**Fig. 3a**). On the basis of this simple model, the Ins-1 loop of Rpn11 folds over the unstructured ubiquitin C terminus, in a similar area to that where AMSH-LP forms the three-stranded sheet. Rpn11 and AMSH-LP thus seem to use the same portions of their Ins-1 regions but very distinct strategies to interact with and stabilize the ubiquitin C terminus in the catalytic groove.

Comparison of our cryo-EM reconstructions for the substrate-free and stalled substrate-bound proteasome revealed that the engagement of ubiquitinated substrate leads to the appearance of a bridging density over the ubiquitin-binding groove of Rpn11 (refs. 22,23) (**Fig. 4a–c**). Docking the Rpn11 crystal structure into the EM maps allowed us to unambiguously assign this bridging density to the Ins-1 loop, which is lifted out of the catalytic groove by ~2.0 Å upon ubiquitin binding (**Fig. 4c**). The observed electron density clearly contradicts the formation of a three-stranded β-sheet with ubiquitin but instead supports our model that the Ins-1 loop of Rpn11 folds over the ubiquitin C terminus. This loop reaching over the catalytic groove is thus reminiscent of another structural feature in AMSH-LP, in which Phe407 of Ins-2 and Asp321 at the tip of the Ins-1 β-sheet fold over the C terminus of a bound ubiquitin (**Fig. 4d**). Consistently with these architectural similarities, mutations of both the Ins-1 loop in Rpn11 and the Phe407 residue in AMSH-LP[20] lead to severe catalytic defects, probably by disrupting the stabilization of the ubiquitin C terminus in the catalytic groove. However, while Phe407 in AMSH-LP forms a stabilizing bridge directly above the isopeptide bond, the Ins-1 loop in Rpn11 is located much further toward the globular fold of ubiquitin (**Fig. 4c,d**). On the basis of the ubiquitin-bound model of Rpn11, the side chain of Glu81 in the Ins-1 loop may form a salt bridge with Arg42 or Arg72 in ubiquitin, and this would explain the 4.3-fold increase in K_m for ubiquitin cleavage by the Rpn11^{E81A} mutant (**Fig. 3a**).

Our structural and mutational data together suggest a mechanism in which the Ins-1 loop functions as a mobile flap that allows a ubiquitin substrate to access the catalytic groove and, upon binding, folds over the ubiquitin C terminus to stabilize it for isopeptide-bond cleavage. Two observations suggest that this loop is intrinsically flexible when not interacting with substrate: (i) defined electron density for the loop appears only in the EM reconstruction of the 26S proteasome stalled on a ubiquitinated substrate, and (ii) *B* factors of the Ins-1 loop in the substrate-free Rpn11 structure are much higher than the average *B* factor for the entire Rpn11–Rpn8 dimer.

Rpn11 has low catalytic efficiency

On the basis of our crystal structure of Rpn11 and the EM reconstruction of the proteasome holoenzyme, Rpn11 lacks important elements that could directly contact and stabilize the Gly-Gly-Lys isopeptide linkage in the active site (**Figs. 3a** and **5a**). In particular, we do not expect the Ins-1

© 2014 Nature America, Inc. All rights reserved.

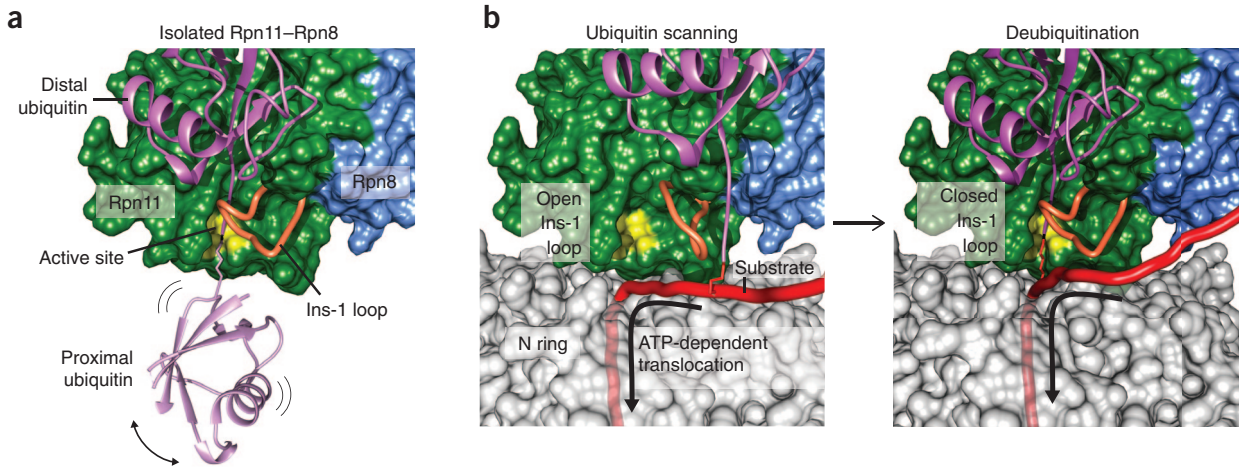

Figure 5 Model for Rpn11-mediated deubiquitination. (**a**) Rpn11 does not contact the proximal side of the isopeptide bond, and this makes its ubiquitin-cleavage activity independent of the linkage type or the identity of the proximal moiety. As a consequence, the isopeptide bond is less stabilized in the Rpn11 active site; this results in slower cleavage compared to that of related DUBs. In this model figure, the diubiquitin was placed into the Rpn11 catalytic groove on the basis of superimposition of Rpn11 and ubiquitin-bound AMSH-LP. (**b**) Because Rpn11 lacks Ins-2 and an extended Ins-1 β-sheet on the proximal side of the catalytic groove, it can function as a promiscuous DUB during ATP-dependent substrate degradation by the proteasome. Rpn11's catalytic residues are positioned directly above the entrance to the processing pore of the base N ring, such that the translocation of substrates pulls attached ubiquitin modifications right into the active site. This ubiquitin-scanning mechanism would be facilitated by the flexible Ins-1 loop, which may function as a flap that allows ubiquitin access to the catalytic groove and folds over the C terminus of a bound distal ubiquitin to stabilize it for cleavage. Owing to the position of the N-ring central pore in line with the Rpn11 catalytic groove, the forceful translocation of substrates into this pore may orient and stabilize the ubiquitin-linked lysines in the Rpn11 active site and thus accelerate isopeptide-bond cleavage.

© 2014 Nature America, Inc. All rights reserved.

loop to interact with the far C terminus of ubiquitin around the isopeptide bond, and Ins-2 is probably precluded from positioning the scissile bond, owing to its contacts with Rpn2. The observation that Rpn11 lacks those specific isopeptide-stabilizing interactions is corroborated by its very low k_{cat} of ~0.3–0.7 min^{-1} for diubiquitin and 1 min^{-1} for ubiquitin-lysine-TAMRA. Rpn11 cleaves Lys63-linked diubiquitin ~134 times more slowly than does AMSH-LP[20], which more strongly stabilizes the isopeptide bond for cleavage, for instance through an active site enclosure by the bridging residues Phe407 and Asp321 (**Fig. 4d**).

Rpn11-mediated deubiquitination during substrate degradation by the proteasome has been shown to be strictly dependent on ATP hydrolysis by the base[17,18]. Interestingly, this degradation-coupled deubiquitination happens at the same rate as the cleavage of ubiquitin-lysine-TAMRA by isolated Rpn11 (1 min^{-1}; ref. 22 and this study), thus suggesting that deubiquitination by Rpn11 represents the rate-limiting step of proteasomal degradation. ATPase-driven polypeptide translocation into the base N ring, located below Rpn11, may pull the isopeptide bond at the base of an attached ubiquitin chain into the Rpn11 active site and thus overcome steric hindrances between the substrate and subunits surrounding Rpn11 in the proteasome context (**Fig. 5b**). The active site architecture of Rpn11 may have been optimized to accommodate highly divergent protein substrates *en route* to the central processing pore and to allow the removal of their ubiquitin modifications concomitantly with degradation, while nonengaged substrates are precluded from deubiquitination.

DISCUSSION

The high-resolution crystal structure of the proteasome Rpn11–Rpn8 heterodimer provides critical insights into the architecture of MPN-domain dimers as well as the mechanisms of Rpn11-mediated substrate deubiquitination at the 26S proteasome. Various ubiquitin-interacting proteins bind to the hydrophobic patch around Ile44 of ubiquitin, and it has so far been assumed that Rpn11 interacts in a similar manner with this patch to bind its substrates for isopeptide cleavage. Remarkably, our crystal structure now reveals that the critical phenylalanine used by related DUBs to bind the ubiquitin Ile44 patch is instead used by Rpn11 to stabilize the heterodimer interface with Rpn8, so that this phenylalanine is inaccessible for ubiquitin binding. It is not ruled out that Rpn11 uses a different, unidentified surface to interact with the Ile44 patch. However, the substantial gain in ubiquitin affinity upon introduction of a phenylalanine at the predicted Ile44-binding site suggests that Rpn11 interacts with ubiquitin in an orientation similar to that of related DUBs, such as AMSH-LP. Rpn11 may use the Ile44 patch of ubiquitin in a different manner resulting in lower affinity and therefore may rely to a larger extent on other conserved interfaces for binding. The original surface for Ile44-patch binding may have been repurposed to form stable interactions with Rpn8 when Rpn11 evolved to become incorporated into the 26S proteasome. These contacts with Rpn8 probably help position Rpn11 over the proteasome central pore and allow translocation-coupled substrate deubiquitination.

For deubiquitination during proteasome degradation, Rpn11 must be able to remove ubiquitin chains from the wide variety of substrates, irrespective of the amino acid sequences surrounding the ubiquitin-linked lysines in these proteins. During its evolution, the enzyme probably accomplished such high promiscuity by eliminating structures that stabilize the isopeptide bond in the direct vicinity of the proximal moiety, or even interact with the proximal moiety itself, and that therefore confer selectivity for certain ubiquitin linkages. In AMSH-LP for instance, the Ins-1 and Ins-2 regions stabilize the Gly-Gly-Lys isopeptide segment, but they also determine the Lys63-cleavage specificity, owing to their interactions with the proximal side of the linkage. Hence, instead of using an extended β-sheet that constitutes one side of the lower catalytic groove, Rpn11 stabilizes its substrates for isopeptide-bond cleavage by folding a flexible Ins-1 loop over the C terminus of the distal ubiquitin (**Fig. 5**). Furthermore, the Ins-2 segment of Rpn11 is removed from the catalytic groove and interacts with Rpn2, which may additionally stabilize the DUB within the proteasome complex. Because Rpn11 is positioned directly above the N ring and even partially occludes the entrance to the central pore, this reduction of protruding structural elements on the proximal

side of its catalytic groove probably also facilitates access of protein substrates to the base-translocation machinery and their ATPase-driven passage underneath Rpn11 while being scanned for ubiquitin modifications. In summary, fewer substrate-stabilizing interactions around the active site appear to make Rpn11 less efficient in isopeptide-bond cleavage but extremely promiscuous for the cotranslocational deubiquitination of highly variable substrates at the proteasome.

METHODS

Methods and any associated references are available in the online version of the paper.

Accession codes. Atomic coordinates and structure factors have been deposited in the Protein Data Bank under accession codes 4O8X (Zn^{2+}-bound Rpn11–Rpn8) and 4O8Y (Zn^{2+}-free Rpn11–Rpn8).

Note: Any Supplementary Information and Source Data files are available in the online version of the paper.

ACKNOWLEDGMENTS

We thank the members of the Martin laboratory for helpful discussions and D. Morgan (University of California, San Francisco) for providing expression constructs for E1 and E2 enzymes. We are also grateful to M. Herzik (University of California, Berkeley) and A. Lyubimov (Stanford University) for help with crystallography data collection and processing. E.J.W. acknowledges support from the US National Science Foundation Graduate Research Fellowship. This research was funded in part by the Searle Scholars Program (A.M.), start-up funds from the University of California, Berkeley Department of Molecular and Cell Biology (A.M.) and the US National Science Foundation CAREER Program (NSF-MCB-1150288 to A.M.).

AUTHOR CONTRIBUTIONS

E.J.W. and A.M. designed experiments; E.J.W. and C.P. expressed, purified and characterized protein variants; and E.J.W. performed X-ray crystallographic studies. E.J.W. and A.M. prepared the manuscript.

COMPETING FINANCIAL INTERESTS

The authors declare no competing financial interests.

Reprints and permissions information is available online at http://www.nature.com/reprints/index.html.

© 2014 Nature America, Inc. All rights reserved.

1. Finley, D. Recognition and processing of ubiquitin-protein conjugates by the proteasome. *Annu. Rev. Biochem.* **78**, 477–513 (2009).
2. Glickman, M.H. & Ciechanover, A. The ubiquitin-proteasome proteolytic pathway: destruction for the sake of construction. *Physiol. Rev.* **82**, 373–428 (2002).
3. Pickart, C.M. Mechanisms underlying ubiquitination. *Annu. Rev. Biochem.* **70**, 503–533 (2001).
4. Xu, P. *et al.* Quantitative proteomics reveals the function of unconventional ubiquitin chains in proteasomal degradation. *Cell* **137**, 133–145 (2009).
5. Saeki, Y. *et al.* Lysine 63-linked polyubiquitin chain may serve as a targeting signal for the 26S proteasome. *EMBO J.* **28**, 359–371 (2009).
6. Thrower, J.S., Hoffman, L., Rechsteiner, M. & Pickart, C.M. Recognition of the polyubiquitin proteolytic signal. *EMBO J.* **19**, 94–102 (2000).
7. Matyskiela, M.E. & Martin, A. Design principles of a universal protein degradation machine. *J. Mol. Biol.* **425**, 199–213 (2013).
8. Saeki, Y. & Tanaka, K. Assembly and function of the proteasome. *Methods Mol. Biol.* **832**, 315–337 (2012).
9. Groll, M. *et al.* Structure of 20S proteasome from yeast at 2.4 A resolution. *Nature* **386**, 463–471 (1997).
10. Groll, M. *et al.* A gated channel into the proteasome core particle. *Nat. Struct. Biol.* **7**, 1062–1067 (2000).
11. Glickman, M.H., Rubin, D.M., Fried, V.A. & Finley, D. The regulatory particle of the *Saccharomyces cerevisiae* proteasome. *Mol. Cell. Biol.* **18**, 3149–3162 (1998).
12. Smith, D.M. *et al.* Docking of the proteasomal ATPases' carboxyl termini in the 20S proteasome's a ring opens the gate for substrate entry. *Mol. Cell* **27**, 731–744 (2007).
13. Beckwith, R., Estrin, E., Worden, E.J. & Martin, A. Reconstitution of the 26S proteasome reveals functional asymmetries in its AAA+ unfoldase. *Nat. Struct. Mol. Biol.* **20**, 1164–1172 (2013).
14. Erales, J., Hoyt, M.A., Troll, F. & Coffino, P. Functional asymmetries of proteasome translocase pore. *J. Biol. Chem.* **287**, 18535–18543 (2012).
15. Zhang, F. *et al.* Mechanism of substrate unfolding and translocation by the regulatory particle of the proteasome from *Methanocaldococcus jannaschii*. *Mol. Cell* **34**, 485–496 (2009).
16. Peth, A., Nathan, J.A. & Goldberg, A.L. The ATP costs and time required to degrade ubiquitinated proteins by the 26 S proteasome. *J. Biol. Chem.* **288**, 29215–29222 (2013).
17. Verma, R. *et al.* Role of Rpn11 metalloprotease in deubiquitination and degradation by the 26S proteasome. *Science* **298**, 611–615 (2002).
18. Yao, T. & Cohen, R.E. A cryptic protease couples deubiquitination and degradation by the proteasome. *Nature* **419**, 403–407 (2002).
19. Inobe, T., Fishbain, S., Prakash, S. & Matouschek, A. Defining the geometry of the two-component proteasome degron. *Nat. Chem. Biol.* **7**, 161–167 (2011).
20. Sato, Y. *et al.* Structural basis for specific cleavage of Lys 63-linked polyubiquitin chains. *Nature* **455**, 358–362 (2008).
21. Beck, F. *et al.* Near-atomic resolution structural model of the yeast 26S proteasome. *Proc. Natl. Acad. Sci. USA* **109**, 14870–14875 (2012).
22. Matyskiela, M.E., Lander, G.C. & Martin, A. Conformational switching of the 26S proteasome enables substrate degradation. *Nat. Struct. Mol. Biol.* **20**, 781–788 (2013).
23. Lander, G.C. *et al.* Complete subunit architecture of the proteasome regulatory particle. *Nature* **482**, 186–191 (2012).
24. Cooper, E.M. *et al.* K63-specific deubiquitination by two JAMM/MPN+ complexes: BRISC-associated Brcc36 and proteasomal Poh1. *EMBO J.* **28**, 621–631 (2009).
25. Estrin, E., Lopez-Blanco, J.R., Chacon, P. & Martin, A. Formation of an intricate helical bundle dictates the assembly of the 26S proteasome lid. *Structure* **21**, 1624–1635 (2013).
26. Echalier, A. *et al.* Insights into the regulation of the human COP9 signalosome catalytic subunit, CSN5/Jab1. *Proc. Natl. Acad. Sci. USA* **110**, 1273–1278 (2013).
27. Sanches, M., Alves, B.S., Zanchin, N.I. & Guimaraes, B.G. The crystal structure of the human Mov34 MPN domain reveals a metal-free dimer. *J. Mol. Biol.* **370**, 846–855 (2007).
28. Cooper, E.M., Boeke, J.D. & Cohen, R.E. Specificity of the BRISC deubiquitinating enzyme is not due to selective binding to Lys63-linked polyubiquitin. *J. Biol. Chem.* **285**, 10344–10352 (2010).
29. Hofmann, K. & Bucher, P. The PCI domain: a common theme in three multiprotein complexes. *Trends Biochem. Sci.* **23**, 204–205 (1998).
30. Wang, B. *et al.* Abraxas and RAP80 form a BRCA1 protein complex required for the DNA damage response. *Science* **316**, 1194–1198 (2007).
31. Sobhian, B. *et al.* RAP80 targets BRCA1 to specific ubiquitin structures at DNA damage sites. *Science* **316**, 1198–1202 (2007).
32. Davies, C.W., Paul, L.N., Kim, M.I. & Das, C. Structural and thermodynamic comparison of the catalytic domain of AMSH and AMSH-LP: nearly identical fold but different stability. *J. Mol. Biol.* **413**, 416–429 (2011).
33. Ye, Y. *et al.* Ubiquitin chain conformation regulates recognition and activity of interacting proteins. *Nature* **492**, 266–270 (2012).

ONLINE METHODS

Expression and purification of Zn^{2+}-free Rpn11–Rpn8 heterodimers. The MPN domains of both *S. cerevisiae* Rpn11 (residues 2–239) and Rpn8 (residues 1–179) were cloned into the pETDuet-1 expression vector with PreScission cleavable N-terminal His_6 and C-terminal StrepII purification tags to make the Rpn11-Rpn8 expression construct. BL21* (DE3) cells were transformed with the Rpn11-Rpn8 expression construct and grown in dYT medium at 37 °C to OD_{600} = 0.6–0.8. Protein expression was induced overnight at 18 °C with 1 mM isopropyl β-D-thiogalactopyranoside (IPTG). Cells were harvested by centrifugation at 6,000*g* for 25 min and resuspended in lysis buffer 1 (30 mM HEPES, pH 7.6, 100 mM NaCl, 100 mM KCl, 0.5 mM EDTA, 1 mM DTT, 10% glycerol and 20 mM imidazole) supplemented with 2 mg/mL lysozyme, benzonase (Novagen), and protease inhibitors (aprotinin, pepstatin, leupeptin and PMSF). All purification steps were performed at 4 °C. Cells were lysed by sonication for 2 min and clarified by centrifugation at 15,000 r.p.m. for 30 min. Soluble cell extract was bound to Ni-NTA agarose resin (Qiagen) and washed with lysis buffer for ~30 column volumes. The bound protein was eluted with a buffer containing 60 mM HEPES, pH 7.6, 100 mM NaCl, 100 mM KCl, 0.5 mM EDTA, 1 mM DTT, 10% glycerol, and 250 mM imidazole. The His_6 and StrepII purification tags were removed by dialysis into PreScission cleavage buffer (50 mM Tris-HCl, pH 7.6, 150 mM NaCl, 1 mM EDTA, and 1 mM DTT) with PreScission protease for 2 h. Uncleaved protein was removed by passage over Ni-NTA agarose. Protein in the flow through was concentrated with a 10K MWCO Amicon Ultra spin filter (Millipore) and purified further by size-exclusion chromatography on a HiLoad 16/60 Superdex 200 pg column (GE Life Sciences) in GF buffer (50 mM HEPES, pH 7.5, 50 mM NaCl, 50 mM KCl, 0.5 mM EDTA, 1 mM DTT, and 10% glycerol). The purified protein was flash frozen with liquid nitrogen and stored at –80 °C.

Purification of Zn^{2+}-bound Rpn11–Rpn8 heterodimers. Cloning and protein expression of the active Rpn11–Rpn8 heterodimer was the same as for the Zn^{2+}-free Rpn11–Rpn8 heterodimer, except that growth medium was supplemented with 150 μM $ZnCl_2$. Cells were harvested by centrifugation at 6,000*g* for 25 min and resuspended in lysis buffer 2 (60 mM HEPES, pH 8.0, 100 mM NaCl, 100 mM KCl, and 10% glycerol) supplemented with 2 mg/mL lysozyme, benzonase (Novagen), and protease inhibitors (aprotinin, pepstatin, leupeptin and PMSF). All purification steps were performed at 4 °C. Cells were lysed by sonication for 1 min and clarified by centrifugation at 15,000 r.p.m. The soluble extract was then bound to Strep-Tactin Superflow Plus resin (Qiagen) and washed with lysis buffer 2 for ~30 column volumes. Protein was eluted with elution buffer 2 containing 60 mM HEPES, pH 8.0, 100 mM NaCl, 100 mM KCl, 10% glycerol and 2.5 mM desthiobiotin. The His_6 and StrepII purification tags were removed by cleavage with PreScission protease for 2.5 h in the elution buffer. After cleavage, the protein was concentrated and further purified by size-exclusion chromatography on a HiLoad 16/60 Superdex 200 pg column (GE Life Sciences) in lysis buffer 2. Fractions containing the purified protein were concentrated, flash frozen in liquid nitrogen and stored at –80 °C.

Ubiquitin expression and purification. Rosetta II (DE3) pLysS *Escherichia coli* cells were transformed with a pET28a vector containing the ubiquitin gene from *S. cerevisiae* under control of a T7 promoter. Cells were grown in Terrific Broth supplemented with 1% glycerol at 37 °C until OD_{600} = 1.5–2.0 and were induced with 0.5 mM IPTG overnight at 18 °C. Cells were harvested by centrifugation, and pellets were frozen at –80 °C. Purification was carried out as described previously[34], but scaled up with minor modifications. The lysis buffer contained 50 mM Tris-HCl, pH 7.6, 0.02% NP-40, 2 mg/mL lysozyme, benzonase (Novagen), and protease inhibitors (aprotinin, pepstatin, leupeptin and PMSF). Cells were lysed by sonication and 20 min incubation at room temperature. 60% perchloric acid was added to a final concentration of 0.5%, and the solution was stirred on ice for a total of 20 min. A 5-mL HiTrap SP FF column (GE Life Sciences) was used for cation-exchange chromatography, and ubiquitin fractions were pooled and exchanged into Ub storage buffer (20 mM Tris-HCl, pH 7.6, and 150 mM NaCl) by repeated dilution and concentration in Amicon Ultra 3000 MWCO spin concentrators (Millipore).

Purification of E1 and E2 enzymes for *in vitro* ubiquitination. Plasmids containing the Ube1, Cdc34, UbcH13, Uev1A, and Ube2S were gifts from the Morgan laboratory. Ube1 was cloned into pET28a, expressed in *E. coli* and purified with ubiquitin-agarose as described[35]. Cdc34 was cloned into pET28a with an N-terminal His_{10} affinity tag, and UbcH13, Uev1A, and Ube2S were cloned into pET28a vectors with C-terminal His_6 affinity tags. All polyhistidine-tagged constructs were grown in dYT at 37 °C to OD_{600} of 0.6–0.8 and were induced overnight at 18 °C with 0.5 mM IPTG. Cells were harvested and resuspended in lysis buffer 3 (50 mM Tris-HCl, pH 8.0, 500 mM NaCl, 20 mM imidazole, and 10% glycerol) supplemented with 2 mg/mL lysozyme, benzonase (Novagen), and protease inhibitors (aprotinin, pepstatin, leupeptin and PMSF) at a ratio of 1:3 cell mass (g)/buffer (mL). Cells were lysed by sonication for 2 min at 4 °C, the lysate was clarified by centrifugation at 15,000 r.p.m. for 30 min, and the soluble extract was bound to Ni-NTA agarose resin (Qiagen) and washed with lysis buffer 3. The bound protein was eluted with lysis buffer 3 plus 250 mM imidazole (500 mM imidazole for His_{10}-Cdc34). The eluate was further purified by size-exclusion chromatography on a HiLoad 16/160 Superdex 75 pg column (GE Life Sciences) in E2 storage buffer (20 mM Tris-HCl, pH 7.5, 150 mM NaCl, 1 mM DTT, and 10% glycerol). UbcH13 and Uev1A Ni-NTA eluates were combined before SEC and eluted as a heterodimer. Concentrations of purified proteins were determined by UV absorbance at 280 nm, and proteins were stored at –80 °C.

Preparation of Lys11-, Lys48- and Lys63-linked diubiquitin. Ubiquitin dimers were synthesized and purified as previously described[36].

Fluorescence-based diubiquitin binding assay. The tryptophan fluorescence of Rpn11 increases upon binding of ubiquitin (which does not contain any tryptophan) and can thus be used as a selective probe to determine the ubiquitin binding affinity. The tryptophan fluorescence of $Rpn11^{V80A}$ was monitored at 30 °C, at an excitation wavelength of 295 nm and an emission wavelength of 330 nm. $Rpn11^{V80A}$ was stored in lysis buffer 2, whereas Lys48-linked diubiquitin was stored in Ub storage buffer. The fluorescence experiments were therefore performed in 30% Ub storage buffer and 70% lysis buffer 2 to make buffer composition consistent for the titration across all ubiquitin concentrations. Fluorescence of 5 μM $Rpn11^{V80A}$–Rpn8 was measured in triplicate at diubiquitin concentrations ranging from 15 μM to 500 μM and fit to a simple binding curve to determine K_d, with Grafit data analysis (Erithacus).

Kinetic analyses of Rpn11 DUB activity. *Diubiquitin cleavage assay.* All diubiquitin cleavage experiments were performed at 30 °C in buffer containing 60 mM HEPES, pH 8.0, 100 mM NaCl, 100 mM KCl and 10% glycerol. The concentration of Zn^{2+}-bound Rpn11–Rpn8 heterodimer was 5 μM for all variants. Initial cleavage rates were measured for eight concentrations of diubiquitin, ranging from 15 to 500 μM (for Rpn11 wild type, D85V, A89F, V78A, S79A, V80A, E81A, Δ78–81, and 78–81A) or from 30 to 700 μM (for Rpn11 E81A and L132A). Cleavage reactions were stopped with 2× SDS-PAGE sample buffer to a final concentration of 3% SDS. Time points for each substrate concentration were analyzed by SDS-PAGE gels stained with SYPRO Ruby (Invitrogen). Monomeric ubiquitin was loaded alongside the cleavage experiments for quantification, and an internal control of single-chain ClpX hexamer was used to normalize for differences in Rpn11 concentration and staining across multiple gels. Gels were imaged on a Typhoon Variable Mode Imager (Amersham Biosciences), with a pixel density of 50 μm/pixel. Monomeric ubiquitin-band intensity was quantified with ImageQuant (GE). Cleavage reactions were repeated three times, and initial rates were fit directly to the Michaelis–Menten equation with nonlinear regression.

Ubiquitin-lysine-TAMRA cleavage assay. Cleavage of ubiquitin-lysine-TAMRA (Boston Biochem) was followed by fluorescence polarization (FP) in buffer containing 50 mM HEPES, pH 8.0, 100 mM NaCl and 100 mM KCl (FP buffer) at 30 °C. Concentrated Rpn11–Rpn8 was buffer-exchanged from lysis buffer 2 into FP buffer with a Micro Bio-Spin 6 chromatography column (Bio-Rad). FP was monitored at 0° and 90° relative to the polarization of the incident beam at an excitation wavelength of 544 nm and an emission wavelength of 574 nm. The limited solubility of ubiquitin-lysine-TAMRA in aqueous buffer precluded the measurement of a complete Michaelis–Menten curve. k_{cat} and K_m were therefore determined by measurements under single-turnover conditions and multiple turnover at ubiquitin-lysine-TAMRA concentrations in the low-micromolar range. For the single-turnover k_{cat} measurement, FP of 100 nM ubiquitin-lysine-TAMRA in the presence of 450 μM wild-type Rpn11–Rpn8 was monitored over 400 s and fitted to a single exponential (Grafit data analysis, Erithacus). Multiple-turnover measurements of ubiquitin-lysine-TAMRA cleavage were conducted in triplicate with 250 nM or 1,250 nM wild-type Rpn11–Rpn8 at 1 μM, 5 μM, and 10 μM ubiquitin-lysine-TAMRA. Cleavage velocities were calculated as described previously[37],

© 2014 Nature America, Inc. All rights reserved.

doi:10.1038/nsmb.2771

with an FP endpoint for completely cleaved ubiquitin-lysine-TAMRA determined after 10-min incubation with 100 nM of the DUB Yuh1. The K_m for Rpn11 cleavage of ubiquitin-lysine-TAMRA was calculated by fitting of the 1 μM, 5 μM, and 10 μM multiple-turnover velocities to a Michaelis–Menten equation and constraining V_{max} (k_{cat}) to the value measured in single-turnover experiments.

Crystal-structure determination of the Rpn11–Rpn8 heterodimer. *Crystallization.* Zinc-free Rpn11–Rpn8 heterodimer was buffer-exchanged into a buffer containing 60 mM HEPES, pH 7.6, 100 mM NaCl and 1 mM TCEP with a Micro Bio-Spin 6 chromatography column (Bio-Rad). Initial crystallization experiments were performed at 18 °C with the hanging-drop diffusion method. A Mosquito liquid-handling robot (TTP Labtech) was used to set about 360 conditions from sparse matrix crystal screens JCSG+ (Qiagen), Wizard I and II (Emerald Bio), Index I and II (Hampton Research) and Crystal Screen I and II (Hampton Research). After optimization of our initial hits, the best crystals of the Zn^{2+}-free Rpn11–Rpn8 complex were obtained from 4-μl hanging drops, for which 2 μl of 5 mg/ml Rpn11–Rpn8 heterodimer was mixed with 2 μl of precipitant solution containing 15% PEG 8000, 12% ethylene glycol and 100 mM HEPES, pH 7.5. The hanging drops were allowed to equilibrate with a 500-μl reservoir of precipitant solution for 4 d at 18 °C. Crystals were soaked for 5 min in a cryoprotectant solution containing 15% PEG 8000, 30% ethylene glycol, and 100 mM HEPES, pH 7.5 before freezing. Crystals of the Zn^{2+}-bound Rpn11–Rpn8 complex were prepared in the same way as for the Zn^{2+}-free crystals, except that the crystals were soaked for 40 min in a cryoprotectant solution containing 15% PEG 8000, 30% ethylene glycol, 100 mM HEPES, pH 7.5 and 500 μM $ZnCl_2$.

Data collection and processing. Diffraction data for the Zn^{2+}-free crystals were collected at a wavelength of 1.075 Å at the NSLS beamline X29A (Brookhaven National Laboratory), and data for the Zn^{2+}-bound crystals were collected at a wavelength of 1.11587 Å at the ALS beamline 8.3.1 (Lawrence Berkeley National Laboratory), both at a temperature of ~100 K. Data were processed with HKL2000 (HKL Research). The structure of the Zn^{2+}-free Rpn11–Rpn8 dimer was solved by molecular replacement with the Phenix suite[38], with structures of Csn5 (PDB 4F7O) and Mov34 (PDB 2O95) as search models. The structures of Csn5 and Mov34 were modified before molecular replacement with Sculptor. The structure of the Zn^{2+}-bound Rpn11–Rpn8 complex was solved by molecular replacement with the Zn^{2+}-free structure as a search model. Iterative refinement, manual model correction and model building were accomplished with Phenix and Coot[39]. The final molecular models have very good stereochemistry (98% Ramachandran favored for both structures, and 0.3% Ramachandran outliers for the Zn^{2+}-free structure) and rotamer orientations, except for the side chain of Rpn11 R100, which, however, was fit into clear electron density. The Zn^{2+}-free complex was refined to an R_{free} of 0.2094, and the Zn^{2+}-bound structure was refined to an R_{free} of 0.1951. Both the Zn^{2+}-free and Zn^{2+}-bound crystals are in the $P4_32_12$ space group with unit-cell dimensions of a = b = 70.405 and c = 198.887, and a = b = 70.296 and c = 198.912, respectively.

34. Pickart, C.M. & Raasi, S. Controlled synthesis of polyubiquitin chains. *Methods Enzymol.* **399**, 21–36 (2005).
35. Ciechanover, A., Elias, S., Heller, H. & Hershko, A. "Covalent affinity" purification of ubiquitin-activating enzyme. *J. Biol. Chem.* **257**, 2537–2542 (1982).
36. Dong, K.C. *et al.* Preparation of distinct ubiquitin chain reagents of high purity and yield. *Structure* **19**, 1053–1063 (2011).
37. Sem, D.S. & McNeeley, P.A. Application of fluorescence polarization to the steady-state enzyme kinetic analysis of calpain II. *FEBS Lett.* **443**, 17–19 (1999).
38. Adams, P.D., Mustyakimov, M., Afonine, P.V. & Langan, P. Generalized X-ray and neutron crystallographic analysis: more accurate and complete structures for biological macromolecules. *Acta Crystallogr. D Biol. Crystallogr.* **65**, 567–573 (2009).
39. Emsley, P. & Cowtan, K. Coot: model-building tools for molecular graphics. *Acta Crystallogr. D Biol. Crystallogr.* **60**, 2126–2132 (2004).

© 2014 Nature America, Inc. All rights reserved.